Ecological Indicators 154 (2023) 110665

Contents lists available at ScienceDirect

Ecological Indicators

journal homepage: www.elsevier.com/locate/ecolind

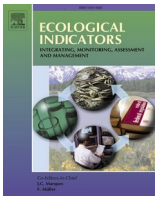

Advancing peatland vegetation mapping by spaceborne imaging spectroscopy

M. Arasumani [a,b,*], Fabian Thiel [a], Vu-Dong Pham [a,b], Christina Hellmann [a], Moritz Kaiser [c], Sebastian van der Linden [a,b]

[a] Institute of Geography and Geology, University of Greifswald, Partner in the Greifswald Mire Centre, Friedrich-Ludwig-Jahn-Straße 16, Greifswald 17489, Germany
[b] Interdisciplinary Centre for Baltic Sea Region Research (IFZO), University of Greifswald, Bahnhofstraße 51, Greifswald 17489, Germany
[c] Michael Succow Stiftung, Partner in the Greifswald Mire Centre, Ellernholzstr. 1/3, Greifswald 17489, Germany

ARTICLE INFO

Keywords:
Remote sensing, PRISMA
Spectral unmixing
Phragmites
Typha
Peatland species mapping

ABSTRACT

Peatlands contribute to a wide range of ecosystem services. They play an important role as carbon sinks in their natural state, but when they are drained, they cause carbon emissions. Rewetting drained peatlands is required to reduce carbon emissions and create new carbon sinks. However, drained peatlands are commonly used as grassland or croplands; therefore, alternative agriculture schemes are required following rewetting. Paludiculture, i.e., agriculture on wet and rewetted peatlands, is an option in these areas after rewetting to produce biomass sustainably. Monitoring of peatland management is challenging, yet needed to ensure a successful rewetting and plantation of, e.g., *Phragmites australis* and *Typha* spp., two plants which are commonly used in paludiculture. Remote sensing is an excellent tool for monitoring the vegetation composition of vast rewetted peatland regions. However, because many peatland species have similar spectral characteristics, such monitoring is ideally based on high-spatial, high-temporal hyperspectral images. Data that complies with all these requirements does not exist on a regular basis. Therefore, we assessed the potential for mapping peatland vegetation communities in the Peene and Trebel river basins of the federal state of Mecklenburg-Western Pomerania, Germany, using multi-date hyperspectral (PRISMA) data. We used regression-based unmixing to map fractions of different peatland vegetation classes. Results were analyzed with regard to the contribution of multi-date observations and, in comparison, to multispectral datasets (Landsat-8/Sentinel-2). Our results showed that different classes are best mapped at different observation dates. The multi-date hyperspectral datasets produced less Mean Absolute Error (MAE = 16.4%) than the single-date hyperspectral images (ΔMAE + 1%), with high accuracies for all classes of interest. Compared to the results obtained with multispectral data from similar acquisition dates and annual spectral-temporal metrics (STM), the results from hyperspectral data were always clearly superior (ΔMAE + 4%). Besides the superior performance during comparisons, our results also indicate that information that can be derived from the hyperspectral data with the regression-based unmixing goes clearly beyond that of discrete classification. With more hyperspectral sensors coming up and an expected higher availability of multi-data hyperspectral imagery, these data can be expected to play a bigger role in the future monitoring of peatlands.

1. Introduction

Peatlands are among the most valuable ecosystems in the world; they contribute to a wide range of critical ecosystem services, e.g., conserving biological diversity (Barthelmes et al., 2015; Parish et al., 2008), regulating water supply (Xu et al., 2018), reducing flood risks (Lupascu et al., 2020), and mitigating climate change (Leifeld and Menichetti, 2018; Strack, 2008). Nevertheless, peatlands are facing threats due to artificial drainage, mainly as a basis for agricultural development, plantations, as well as urban spread and industrial development (Dise, 2009; Roucoux et al., 2017).

Drainage systems were developed in peatlands for agricultural production since centuries; as a result, about 50% of the peatlands in the European Union are degraded with >90% of peatlands in Germany

* Corresponding author.
E-mail addresses: arasumani.muthusamy@uni-greifswald.de, arasustat@gmail.com (M. Arasumani).

https://doi.org/10.1016/j.ecolind.2023.110665
Received 17 March 2023; Received in revised form 2 June 2023; Accepted 12 July 2023
Available online 24 July 2023

being degraded (Joosten et al., 2017; Tanneberger et al., 2021).

Peatland degradation has various severe impacts on the ecosystem (Fluet-Chouinard et al., 2023). One of the most critical ecosystem services provided by peatlands is carbon sequestration and storage. Peatlands cover only 3% of the world's land area (Parish et al., 2008), yet they store more carbon than any other ecosystem on the planet (500 Gt carbon); additionally, they contribute to the annual sequestration of around 0.37 Gt of CO_2 (Joosten et al., 2016). On the other hand, peatlands that have been drained and degraded are the cause of approximately 2 Gt of CO_2 equivalents per year of global carbon emissions (Tanneberger et al., 2022; Joosten, 2010). Drained peatlands also increase the frequency and extent of peat fires (Kettridge et al., 2015; Schulte et al., 2019), potentially leading to additional carbon emissions. Furthermore, the reduction and degradation of peatlands decrease native species abundance (Lehosmaa et al., 2017); for example, Fraixedas et al. (2017) reported that 40% of peatland bird populations were reduced in northern Europe. Similarly, bird populations were affected in north-eastern Germany (Görn et al., 2015). Drainage and related degradation also cause changes in the natural sediment trapping property, hence, soil erosion (Tuukkanen et al., 2016) as well as increasing acidity (Saarinen et al., 2013).

In recent years, the importance of peatlands to society and the ecosystem has been widely acknowledged (Bain et al., 2011), and their roles regarding biodiversity, flood mitigation, and especially carbon storage are now well understood (Parish et al., 2008). Hence, the rewetting of drained peatlands is nowadays primarily initiated to control greenhouse gas emissions and reduce net carbon loss (Günther et al., 2020) but also to support ecosystem services in general (Curtis et al., 2014; Kimmel and Mander, 2010). In addition, peatland rewetting can reduce fire risk by increasing the moisture content (Sirin et al., 2020) and aid in boosting biodiversity values (Görn and Fischer, 2015; Görn et al., 2015; Hoffmann et al., 2018).

Rewetted peatlands can either be left unused as nature protection areas or used for sustainable biomass production on wet soils, i.e. as so-called "paludiculture" (Tanneberger et al., 2022). In both scenarios, carbon emissions are reduced, the peat body is preserved, peat can be accumulated under favourable conditions, and other ecosystem services are supported, e.g., biomass production or water purification (Günther et al., 2020; Tanneberger et al., 2022; Vroom et al., 2018). The biomass produced by paludiculture is, depending on the species, mainly utilized as animal fodder, to produce energy, for building materials, including roof thatching, and packaging in north-eastern Germany.

In order to achieve carbon neutrality, the Paris Agreement mandates that 500,000 km^2 of drained peatlands shall be rewetted globally before 2050–2070 (Kreyling et al., 2021). In Mecklenburg-Western Pomerania, about 26,000 ha of peatlands were rewetted (MLU 2017). Nevertheless, rewetting peatlands can take years to decades (Pouliot et al., 2011). Therefore, constant monitoring is necessary to determine whether the process is successful or not (Knoth et al., 2013).

For north-eastern Germany, most rewetting activities relate to fen peatlands. Paludiculture on such rewetted fen peatlands is still in its early days, and besides the utilization as wet grassland, experiments with potential species include the plantation of *Phragmites australis* (Common Reed) and *Typha* spp. (Cattail). The success of the biomass production of paludiculture crops depends on the rewetting status, such as water level, and nutrient conditions, which are species-specific (Haldan et al., 2022). In addition, dry conditions may alter the vegetation composition, which may lead, for example, to shrub encroachment in peatlands (Wichtmann and Schäfer, 2007). Thus, the abundance and composition of species can be used as an indicator for the success of fen peatland rewetting, and vegetation remote sensing may function as a reliable proxy for rewetting success (Beyer et al., 2021).

Distinguishing vegetation types on wet and rewetted peatlands with remote sensing imagery is always challenging (Krankina et al., 2008; Lees et al., 2018). Although rewetted fen peatlands show similarities to a cropland-grassland mosaic, they differ in some respects, which makes a clear delineation of surfaces and disentangling sub-pixel components more challenging: vegetation such as *P. australis*, *Typha* spp. and wet grassland experience phenology, yet the relatively high share of remnant dry vegetation is not necessarily fully and continuously harvested, partly due to complicated access. Especially in areas without regular harvest, a mix of non-photosynthetically active (NPV) and green vegetation (GV) co-exists with a high share of background signal with varying shadow and water fractions. Moreover, small-scale variations in the water and, hence, temperature regimes lead to offsets in phenology and, this way, additional changes in the appearance of the surfaces in Earth observation data. However, we can resolve these difficulties by using multi-date remote sensing images that can accurately map the peatland vegetation communities using phenological variation in different seasons much better than single-date imagery. Multi-date imagery, however, can only be provided by spaceborne systems, which bring along 10–30 m spatial resolutions for freely and regularly available data. At such scales, *P. australis* and *Typha* spp. occur intermixed with other peatland species and background classes; therefore, sub-pixel classification appears more suitable than per-pixel classification to detect the respective cover fractions.

In principle, an accurate mapping of vegetation communities on rewetted areas is possible using very high spatial resolution multispectral data obtained from an Unmanned Aerial Vehicle (UAV) (Abeysinghe et al., 2019; Beyer et al., 2019; Higgisson et al., 2021; KopeŁ et al., 2016; Steenvoorden et al., 2022). Furthermore, airborne hyperspectral images can be used (Elmer et al., 2021). But, capturing multi-date remote sensing images from UAVs and airborne systems at a landscape level is critical in terms of time, organization or cost, and pre-processing efforts.

Some studies have employed commercial high-resolution multispectral images for mapping peatland species. For example, Ghioca-Robrecht et al. (2008) used multi-date QuickBird imagery for mapping *Typha* spp. and *P. australis*, but they faced misclassification errors due to the absence of shortwave-infrared (SWIR) bands. Landsat data covers the SWIR; nevertheless, the classification may suffer from spectral ambiguity at the combined spectral and spatial resolution of Landsat (Brown et al., 2007). Regardless, Landsat annual or seasonal spectral-temporal metrics may be useful for detecting vegetation types using phenological fluctuation across time (Okujeni et al., 2021).

Data from imaging spectrometers with high spectral resolution from the visible to the SWIR domain are useful for differentiating peatland vegetation communities (McPartland et al., 2019) and such data will play a more important role in the future with the currently accessible spaceborne hyperspectral data from Hyperspectral Precursor and Application Mission (PRISMA — Loizzo et al., 2018), Environmental Mapping and Analysis Program (EnMAP — Guanter et al., 2015) and the upcoming Copernicus Hyperspectral Imaging Mission for the Environment (CHIME) and Surface Biology and Geology (SBG) missions with quasi-continuous spectral coverage between 400 and 2500 nm (nm). The combination of these spaceborne hyperspectral sensors, particularly when used in conjunction, will offer a series of multi-date observations that prove valuable for studying the growing season of peatland vegetation.

Recently, PRISMA data have been used for mapping forest types (Vangi et al., 2021) and crop classification (Pepe et al., 2020), but to the best of our knowledge, PRISMA data have not been explored for unmixing peatland species. We found one study using 30-m hyperspectral data from the Earth-Observing One (EO-1) Hyperion for mapping related peatland vegetation, i.e. *P. australis* in coastal wetlands, with per-pixel classification (Pengra et al., 2007). However, for the monitoring of peatland rewetting activities, a discrete 30-m scale appears too coarse and per-pixel classification hence not useful.

In the presented study, we test the two hypotheses that i) the high spectral information content of PRISMA data allows for more accurate sub-pixel mapping and, hence, compensates for the limited spatial resolution of the image data and ii) observations from multiple dates further improve the map accuracy. This way, we investigate the

potential contributions of new or future data from spaceborne imaging spectrometers to monitoring peatlands. To test our hypothesis, we use the concept of regression-based unmixing with synthetic training data (Okujeni et al., 2013). The approach was developed for sub-pixel mapping of urban areas with (simulated) EnMAP-data and showed the added value of the hyperspectral information compared to multispectral Landsat data of the exact spatial resolution (Okujeni et al., 2015). The approach proved reliable and accurate in several follow-up studies and has been more frequently used for the analysis of vegetation type cover fractions at the sub-pixel scale with hyperspectral and multispectral data (Borges et al., 2022; Cooper et al., 2020; Stanimirova et al., 2022). Previous research by Okujeni et al. (2021) demonstrated the capability of utilizing imagery from multiple dates. Consequently, this approach appears highly suitable for our objective of mapping rewetted fen peatlands in the state of Mecklenburg-Western Pomerania, located in north-eastern Germany, by leveraging multi-date, spaceborne imaging spectroscopy data.

We ask the following research questions (RQ),

1) How far do multi-date observations contribute to more accurately quantifying peatland vegetation composition?
2) To what extent does the additional spectral information in imaging spectroscopy data support the mapping of peatland vegetation communities compared to multispectral information?

2. Methods

2.1. Study area

For this research, we selected rewetted percolation fens located in the valleys of the Peene and Trebel rivers in Mecklenburg-Western Pomerania, Germany. The study area spans from 53°49′N to 53°59′N latitude and 12°53′E to 13°1′E longitude (Fig. 1). It corresponds to the area covered by three flightlines from airborne image acquisition (see section 2.2.3). The study area experiences an average annual air temperature of 9.2 °C and an average annual rainfall of 583 mm at the nearby weather station of Teterow for the period of 1991–2020 (Deutscher-Wetterdienst, 2023). The fens in the Peene and Trebel river basins were formed during the Holocene as a result of the meltwater from the last glacial period (Succow, 1971). These fens possess an exceptional flora typically associated with fen ecosystems (Görn et al., 2015; Hennicke, 2001). The Peene riverine peatland area is of international importance and in large parts protected within the NATURA 2000 network (Hoffmann et al., 2018). Since the 1960 s, several parts of the peatlands in the Peene river valley were heavily drained and used as grassland. However, since 1992 the peatlands along the Peene river's banks have been partly rewetted in order to accomplish biodiversity conservation goals (Hoffmann et al., 2018; Timmermann et al., 2009; Zerbe et al., 2013).

The study area is covered by peatland plants such as *Phalaris arundinacea* (Reed Canary Grass), *Carex* spp. (Sedges), *Phragmites australis* (Common Reed) and *Typha* spp. (Cattail) (Fig. 2), as well as other landcover categories, including forests, non-wet grasslands, wet grasslands, shrublands, water bodies, croplands and settlements. In our study area, peatland species can be found in both unmanaged nature reserves and wet agriculture.

2.2. Image data

To investigate the surplus of multi-date hyperspectral spaceborne imagery, we used PRISMA data from three acquisition dates and created different products (Section 2.2.1) for the regression-based unmixing

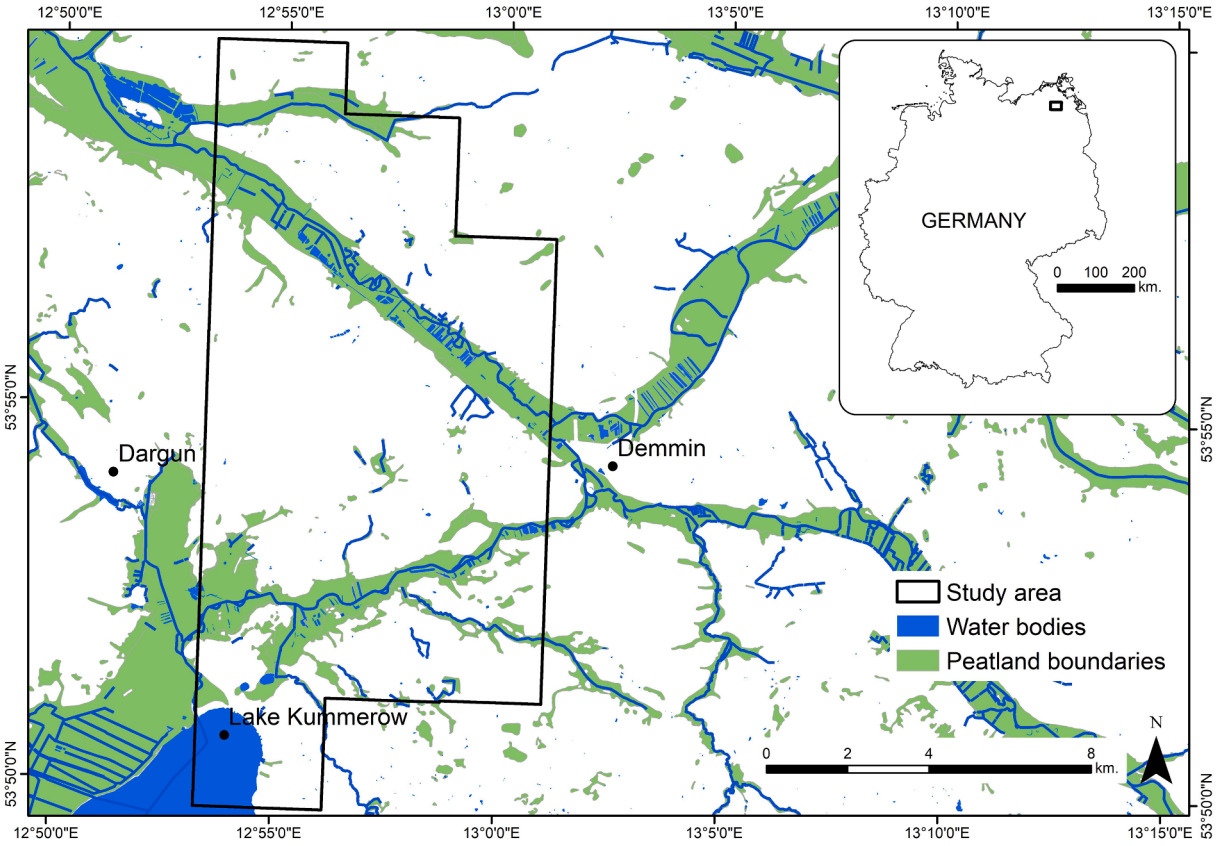

Fig. 1. Study area map – peatlands around the Peene and Trebel rivers, north-eastern Germany. < Source: Waterbody boundaries were obtained from OpenStreetMap, and peatland boundaries were provided by the State Office of the Environment, Nature Conservation, and Geology (LUNG), Mecklenburg-West Pomerania.

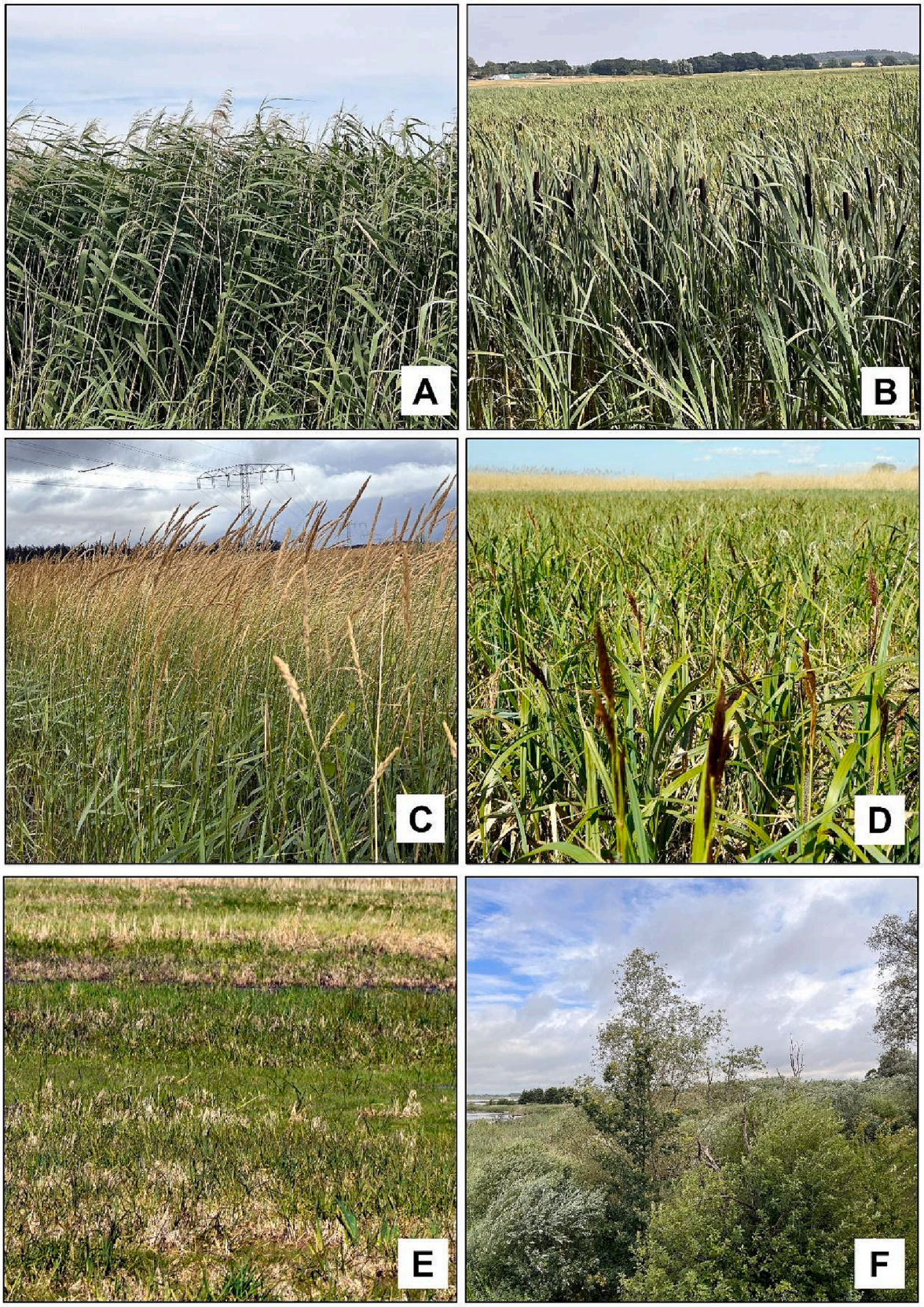

Fig. 2. Field photographs – A) *P. australis*, B) *Typha* spp., C) P. arundinacea, D) Carex spp., E) Wet grasslands and F) Shrublands.

approach (Section 2.4). The results were compared to different products obtained from combined Landsat-8 and Sentinel-2 imagery (Section 2.2.2). We also incorporated airborne hyperspectral data from the Airborne Visible Infrared Imaging Spectrometer – Next Generation (AVIRIS-NG), which offers higher spatial and spectral resolution (Section 2.2.3). This data was ingested to create a classification map, which was later used to validate the unmixing results. Please refer to Fig. 3 for an overview of all image data pre-processing steps and the various products utilized in the experiments.

2.2.1. *Hyperspectral data acquisition and pre-processing*

We obtained the PRISMA Level 2D cloud-free datasets for 19 April, 16 June, and 13 August 2021 (Fig. 3 & Fig. 4), from the Italian Space Agency (ASI). The PRISMA data have a medium spatial resolution (30 m) and high spectral resolution (12 nm) for 239 bands within the spectral range from 400 to 2505 nm. The Level 2D PRISMA datasets were already orthorectified, atmospherically corrected, and delivered in he5 format. We converted the PRISMA datasets into TIFF format and removed the water absorption and bad bands (1–5, 103–113, 147–164 and 225–234) using the EnMAP-Box (EnMAP-Box, 2019); finally, we used 190 spectral bands for the fraction mapping. The multitemporal PRISMA data had geolocation offsets; therefore, we co-registered them with PlanetScope next-generation images using AROSICS (Scheffler et al., 2017).

2.2.2. *Multispectral data acquisition and pre-processing*

To evaluate the surplus of the hyperspectral information, we included time series of multispectral data from the same period. We obtained Sentinel-2 (S2) and Landsat-8 (L8) level-1 data from the European Space Agency (ESA) and the United States Geological Survey

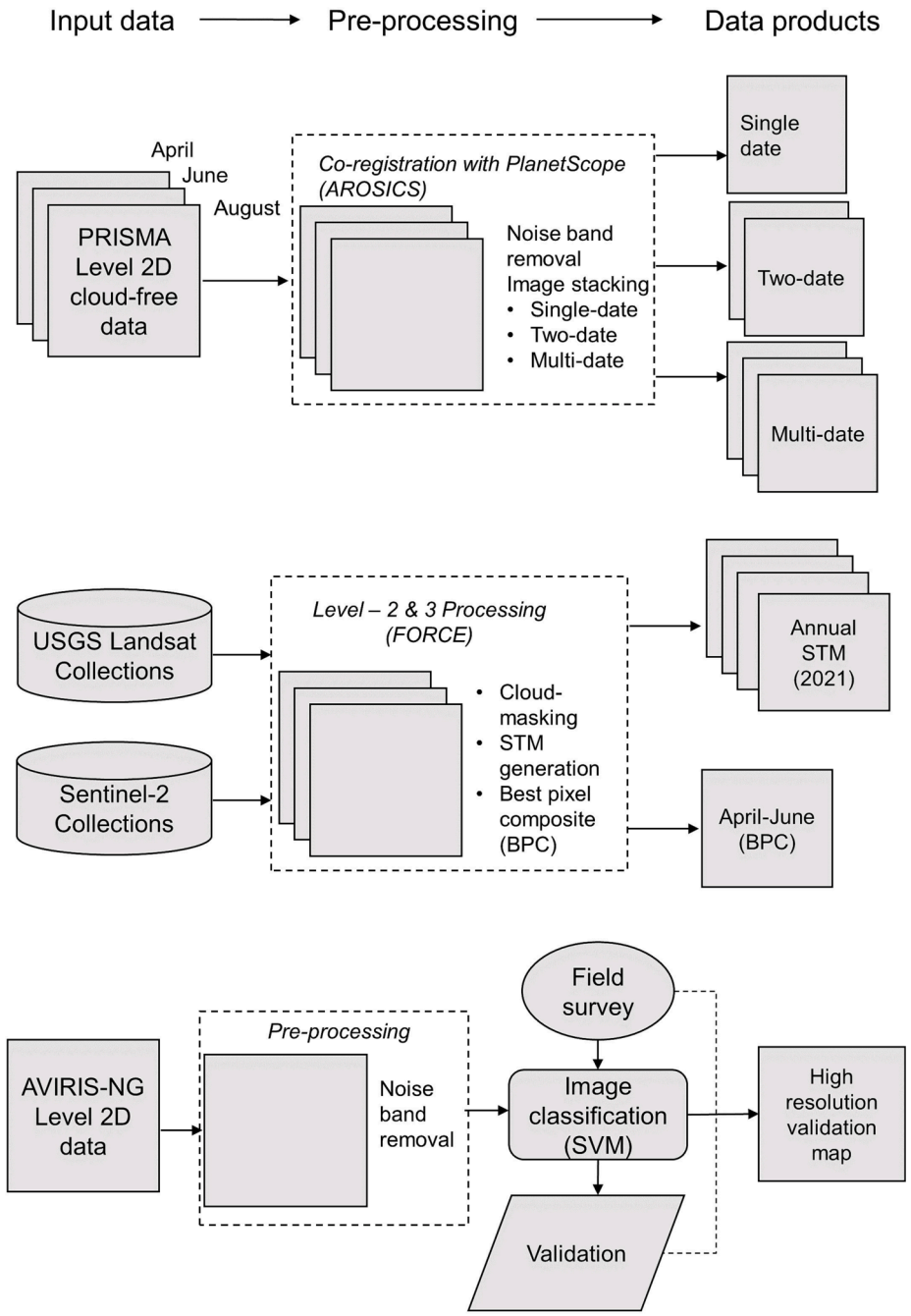

Fig. 3. Flowchart showing all image data sources, the applied pre-processing steps and the resulting data products used during the analysis.

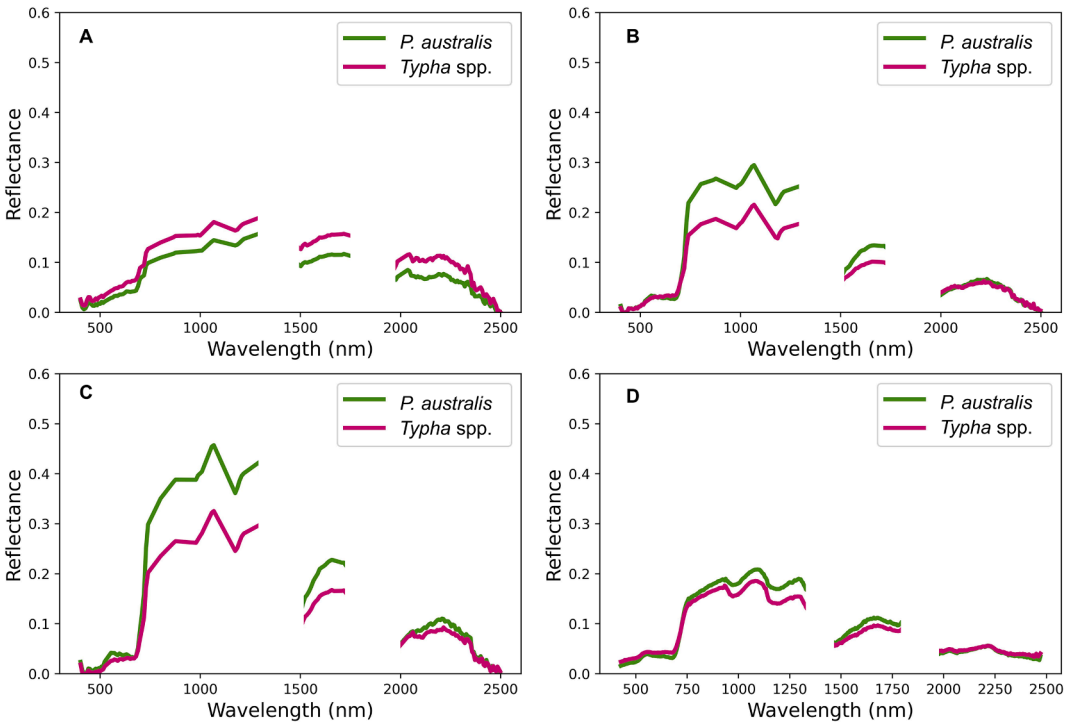

Fig. 4. Mean spectral signatures of *P. australis* and *Typha* spp. – A) PRISMA – acquired in 19 April 2021, B) PRISMA – acquired in 16 June 2021, C) PRISMA – acquired in 13 August 2021 and D) AVIRIS-NG – acquired in 30 May 2021.

(USGS), respectively, for the period from January 2021 to December 2021. We downloaded all images with a cloud cover of less than 75%. Before further investigation, we pre-processed the images and converted them to level-2 data (Fig. 3). This pre-processing encompassed cloud and cloud shadow masking, following the methodologies proposed by Frantz et al. (2018) and Zhu and Woodcock (2012). Additionally, we applied corrections for topographic effects, atmospheric influences, bi-directional reflectance distribution function, and adjacency effects. Furthermore, we co-registered the S2 images with L8 data to ensure spatial alignment. Sentinel-2 images were resampled to 30 m spatial resolution to match the spatial and spectral resolution of L8. All of the pre-processing tasks for both S2 and L8 data were carried out using the Framework for Operational Radiometric Correction for Environmental Monitoring (FORCE) developed by Frantz (2019).

The combined datasets of S2 and L8 lead to high temporal coverage (Griffiths et al., 2019). Still, relatively high cloud coverage over the study region in 2021 limited the number of available scenes. Therefore, we used FORCE to generate best pixel composite (BPC) for April-June in order to allow for comparison with the available PRISMA data (no spatially continuous and cloud-free S2/L8 data for August available). Moreover, we created spectral-temporal metrics (STM) from the combined S2/L8 data for the entire year 2021 for a comparison of the higher spectral content of PRISMA data with the higher temporal content of S2/L8 (Okujeni et al., 2021). STM constitute descriptive statistics on all available clear sky observation for a pixel in a defined time period (Frantz, 2019). This way, not only best pixel values but also the variation throughout the year is used for the comparison, and hence, the variation in reflectance of the temporally higher-resolved multispectral sensors is taken into account. As STM, we calculated the 25th, 50th, and 75th percentile for the S2 and L8 Blue, Green, Red, NIR, SWIR-1, and SWIR-2 bands.

2.2.3. AVIRIS-NG airborne data, pre-processing and classification

We procured three AVIRIS-NG surface reflectance flightlines acquired on 31 May 2021 as part of the European Space Agency (ESA) CHIME campaign (https://ares-observatory.ch/esa_chime_mission_2021/). The area covered by the three adjacent flightlines constitutes the selected study area. The AVIRIS-NG data have a high spatial resolution (5.8 m) and spectral resolution (5 nm) with spectral ranges from 380 to 2510 nm (Fig. 4D). We mosaicked the AVIRIS-NG scenes and subsequently removed the water absorption and bad bands (1–10, 194–210, 286–316, 319, 325–329 and 420–425) from the dataset; in the end, we used 355 spectral bands for the image classification. For the classification, we used 441 training points that were collected. The AVIRIS-NG data were classified into eleven distinct landcover types – *P. australis*, *Typha* spp., *P. arundinacea*, *Carex* spp., forest, non-wet grasslands, wet grasslands, shrublands, water bodies, croplands and settlements using Support Vector Machine (SVM) with radial basis function and parameter grid search. The accuracy of the AVIRIS-NG classified map was validated using an additional set of 356 independent ground truth points.

The LC classification from the AVIRIS-NG data product provided high overall accuracy (90.4%) with well-balanced producer's and user's accuracies (>87%) for the classes of *P. australis*, *Typha* spp., shrublands, wet grasslands, and water (Table 1).

Table 1
Classification accuracies based on the AVIRIS-NG data product. Values for target classes of the fraction maps appear bold. (*Note that *P. arundinacea* and *Carex* spp. have later been combined into the wet grasslands class for the purpose of unmixing medium-resolution images).

Landcover class	User accuracy [%]	Producer accuracy [%]
P. australis	**93**	**87**
Typha spp.	**90**	**90**
Shrublands	**96**	**93**
Wet grasslands	**93**	**93**
Water bodies	**100**	**93**
P. arundinacea	**80**	**86**
Carex spp.	**70**	**86**
Forest	97	96
Croplands	96	83
Non-wet grasslands	80	90
Settlements	87	93

2.3. Field data collection

In our study sites, the different peatland vegetation communities are often intermixed. We identified *P. australis* and *Typha* spp. in larger patches (>30×30 m), which could be used for model training, whereas *P. arundinacea* and *Carex* spp. are mostly dispersed or scattered (less than 20×20 m) and surrounded by vegetation from the wet grassland class. Therefore, we did not find a pure reference area of 30x30 m of *P. arundinacea* and *Carex* spp. pixels and we included these species into the wet grassland category for the unmixing of medium-resolution hyperspectral and multispectral datasets. We collected 98 reference areas with homogeneous vegetation cover in the field for *P. australis* and *Typha* spp., shrublands, wet grasslands and water to be used in the later training of the mapping algorithm. Furthermore, using Google Earth, 54 reference areas were created for training the background class (settlements, croplands, forests and grasslands) based on the field knowledge. Then, we created a spectral library (see next sub-section) based on the ground truth training points and the reflectance profiles from the corresponding pixels in the hyperspectral and multispectral datasets.

2.4. Regression-based unmixing

The regression-based unmixing method with synthetically mixed training data from spectral libraries (Okujeni et al., 2013) was used to map the fractions of *P. australis*, *Typha* spp., shrublands, wet grasslands and water bodies using the single and multi-date hyperspectral and multispectral datasets (Fig. 5). Fraction mapping is performed using machine learning regression. For training the regression model, reflectance profiles representing different class fractions are synthetically created by weighted averaging of two or three LC types. The weights are then used as labels representing the cover fraction as target variables during the regression training (see Cooper et al., 2020 for a detailed description of the approach). We generated synthetic training data from the spectral library (see section 2.3); we created 1000 synthetic training samples for each class. Subsequently, each synthetically mixed spectral signature was randomly created according to the following procedure: (a) we assigned a value of a 50% chance for a two-class mixture, a 40% chance for a three-class mixture, and a 10% chance for a four-class mixture based on field knowledge and initial experiments, (b) a target class of the original library signature was randomly selected and then assigned to create the synthetically mixed spectral signature. This step assured the inclusion of a target class signature. After that, additional library signatures were randomly selected based on class likelihoods, which were chosen by the proportionate representation of each class entry in the spectral library; this procedure ensured the completion of the synthetically mixed feature, (c) then, random mixing fractions

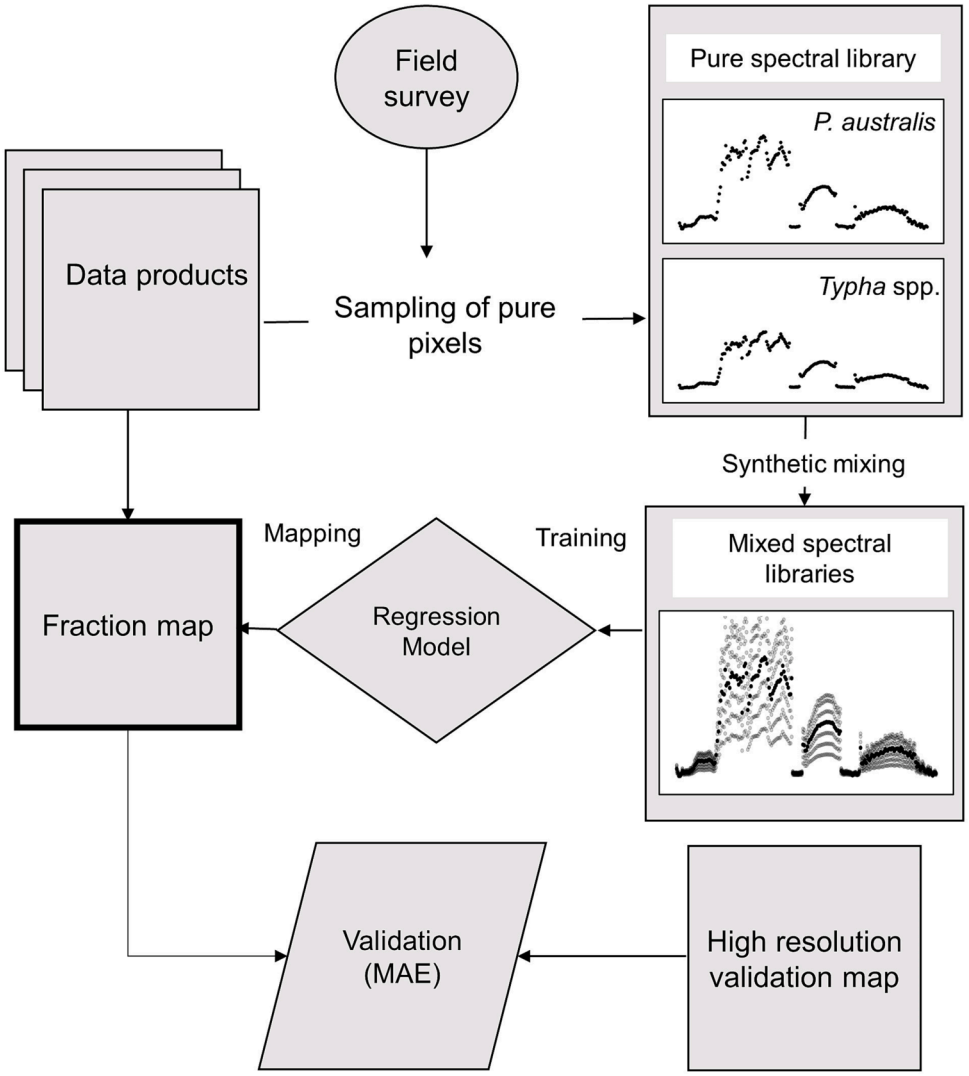

Fig. 5. Workflow for mapping peatland vegetation communities using a regression-based unmixing approach with hyperspectral and multispectral data products.

ranging from 0% to 100% were assigned to the respective spectra, with a sum-to-unity constraint. Furthermore, we included pure library spectra in each synthetic training dataset and assigned mixing fractions of 100% or 0% to library signatures from the target and non-target classes, respectively. We used the Light Gradient Boosting Machine (LightGBM) regression algorithm for fraction mapping (Ke et al., 2017). The LightGBM approach is relatively fast while ensuring high accuracy at the same time (Ke et al., 2017). The creation of the spectral library and fraction mapping was performed using the EnMAP-Box (EnMAP-Box, 2019).

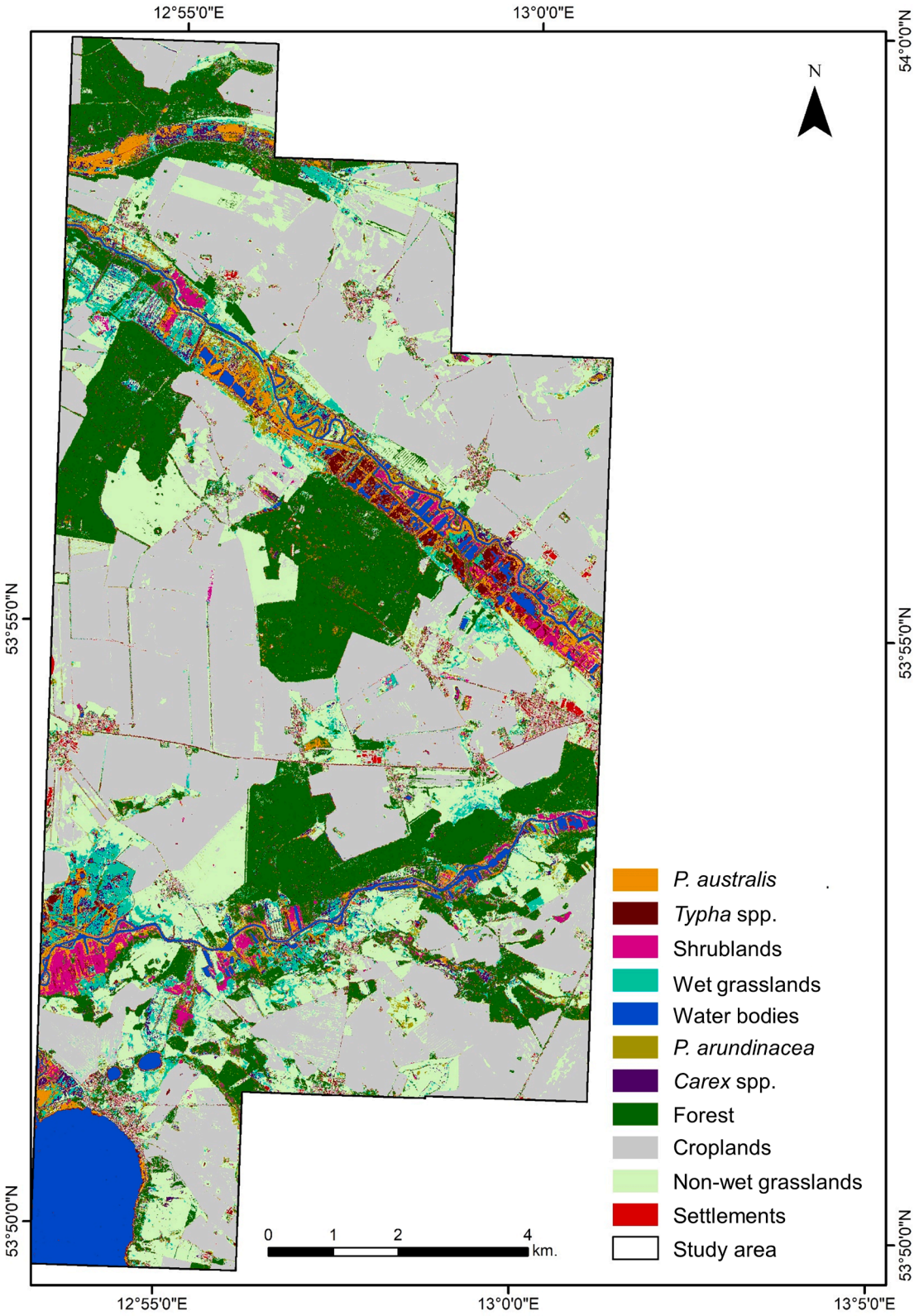

Fig. 6. The very high resolution classification map of peatland vegetation communities produced based on the AVIRIS-NG data with 5.8 m pixel size (*Note that the fractions derived from the medium resolution images were validated using this data).

2.5. Validation

LC fractions at the sub-pixel scale require spatially highly resolved LC information for validation. It is challenging to produce validation data of peatland fractions by field surveys because of the water depth and variety of mixed species in peatlands. However, high spatial resolution classification outcomes could also be an alternative (Atzberger and Rembold, 2013; Ge, 2013; Ge et al., 2016; Kattenborn et al., 2019). Thus, we used the high resolution classification map from the AVIRIS-NG data product (see Section 2.2.3) that was 27 times higher in spatial resolution to validate the fraction maps from the PRISMA and multispectral datasets (Fig. 6). Based on this information, we created the Mean Absolute Error (MAE) from a pair-wise comparison of results from the regression model with the pixel-wise aggregated classification map from AVIRIS-NG. In order to obtain a representative sample, we used a stratified approach and randomly selected 150 pixels for each class.

3. Results

3.1. Single-date vs. multi-date hyperspectral unmixing

While comparing single-date unmixing results from PRISMA data, the April and June datasets produced the overall best results, whereas the August dataset performed worst (see Table 2 and Fig. 7). The classes of high interest (*Typha* spp. and *P. australis*), performed differently over time, for example, *Typha* spp. fraction results were best in June (MAE = 15.05%) as April and August's datasets produced higher errors (ΔMAE + 2%). The April dataset produced the best fraction results of *P. australis* (MAE = 18.73%; June ΔMAE + 2%, August ΔMAE + 2%). With regard to the other classes, the MAEs also varied between months, and the PRISMA data from April led to the highest accuracies for wet grasslands, and data from June produced the best accuracy for the water class.

The two-date combination with the highest accuracy was obtained from the April-June datasets (MAE = 16.41%) when compared to other combinations (see Table 2 and Fig. 7). The combination of June and August was the only two-date combination performing slightly worse than one single-date combination (i.e., April). The April-June (MAE = 14.94%) and June-August (MAE = 15.26%) datasets produced best fraction results of *Typha* spp., while the April-August data produced the best results for mapping *P. australis* fractions (MAE = 17.98%). The April-June datasets generated the best results for shrublands (MAE = 15.49%).

The three-date combination (April-June-August) yielded less error (MAE = 16.69%) compared to the results of all previous combinations, except for the results from the April-June datasets (Fig. 7). We also noticed that the three-date dataset produced the best results for both *P. australis* (MAE = 18.26%) and *Typha* spp. (MAE = 15.34%), in contrast to other combination datasets, which produced the best results for *Typha* spp. but not for *P. australis* and vice versa.

Scatter plots with the estimate and reference fractions per class (Fig. 7; see S1 for a complete set of scatter plots) show the distribution of fraction values. First of all, it can be seen that a high share of pixels of multiple LC with a full range of fractions consists in the reference data and that such fractions are also mapped at full range by the regression-based unmixing. For all model results, the R^2 >0.5 indicates a correlation with the quantitative reference information. Better performing models (with R^2 >0.65 or MAE <18%) appear to clearer follow the 1:1 line when regarding the point distribution and the linear function fitted to the reference and prediction.

3.2. Hyperspectral vs. Multispectral data unmixing

The overall MAE for both results derived from multispectral data were clearly above 20% and hence worse than all results from the hyperspectral data. The differences in MAE were at least 2.2% (compared to PRISMA August) and 3.5–4.5% for most comparisons (See Table 2 and Fig. 7).

The maps produced from hyperspectral (Fig. 8) and multispectral data (Fig. 9) show similar patterns, especially in areas where peatland patches are widespread. However, when using hyperspectral data, the mixtures of *P. australis* and *Typha* spp. were clearly predicted compared to multispectral data that slightly overpredicted the *P. australis* and wet grasslands fractions (Fig. 7).

Fig. 10 shows a subset of peatland species fraction maps created using hyperspectral April-June data (left) and multispectral April-June (BPC; right) in comparison to the aggregated results from the AVIRIS-NG classification (center). The fraction of *Typha* spp. (red) in the hyperspectral was almost identical to the validation data. However, *Typha* spp. fractions were overestimated when using multispectral data. In contrast to multispectral data, results from the hyperspectral data show the rather linear features of *P. australis* (green) in the mosaic of *Typha* spp, where they appear as brown, indicating a less differentiated regression result. The water fraction near *P. australis* was accurately detected by the hyperspectral data, but it was overestimated by the multispectral data as *Typha* spp.

Fig. 11 depicts a subset of wet grasslands, shrublands, and water maps derived from hyperspectral April-June and multispectral April-June (BPC) data. The hyperspectral data's wet grasslands fraction nearly matched the validation data. However, multispectral data underestimated the fraction of wet grasslands. The shrublands fraction from hyperspectral data was slightly matched with the validation data, but in some areas, the fraction was overestimated, whereas multispectral data produced results that differed from the validation data.

4. Discussion

Systematic monitoring of the abundance of peatland vegetation communities is essential for understanding the success of rewetting activities. Therefore, identifying the vegetation composition of various peatland species with high spatial resolution is critical for the sustainable long-term management of peatland and its biodiversity. Hence, deriving highly accurate information requires high spatial resolution images and sufficient spectral or temporal coverage to differentiate spectrally ambiguous vegetation types. However, spaceborne sensors with high spectral and temporal information content only have medium spatial resolutions of 10–30 m pixel size. Therefore, monitoring with

Table 2
Mean Absolute Errors (MAE; in % fraction cover) of unmixing results from the hyperspectral and multispectral datasets.

Datasets	*Typha* spp. (MAE %)	*P. australis* (MAE %)	Shrublands (MAE %)	Wet grasslands (MAE %)	Water (MAE %)	Average (MAE %)
PRISMA April	16.86	18.73	17.37	**17.99**	15.59	17.31
PRISMA June	15.05	20.85	17.52	19.96	**13.82**	17.44
PRISMA August	17.95	20.96	19.16	20.36	15.91	18.87
PRISMA April-June	**14.94**	18.99	**15.49**	18.26	14.38	**16.41**
PRISMA April-August	16.43	**17.98**	16.83	18.63	15.08	16.99
PRISMA June-August	15.26	19.47	17.9	20.45	13.57	17.33
PRISMA April-June-August	15.34	18.26	16.06	19.81	13.99	16.69
L8 + S2 (April-June BPC)	19.16	22.36	21.14	22.69	19.91	21.05
Landsat-8 + Sentinel-2 (STM)	22.16	23.78	20.87	22.17	20.02	21.8

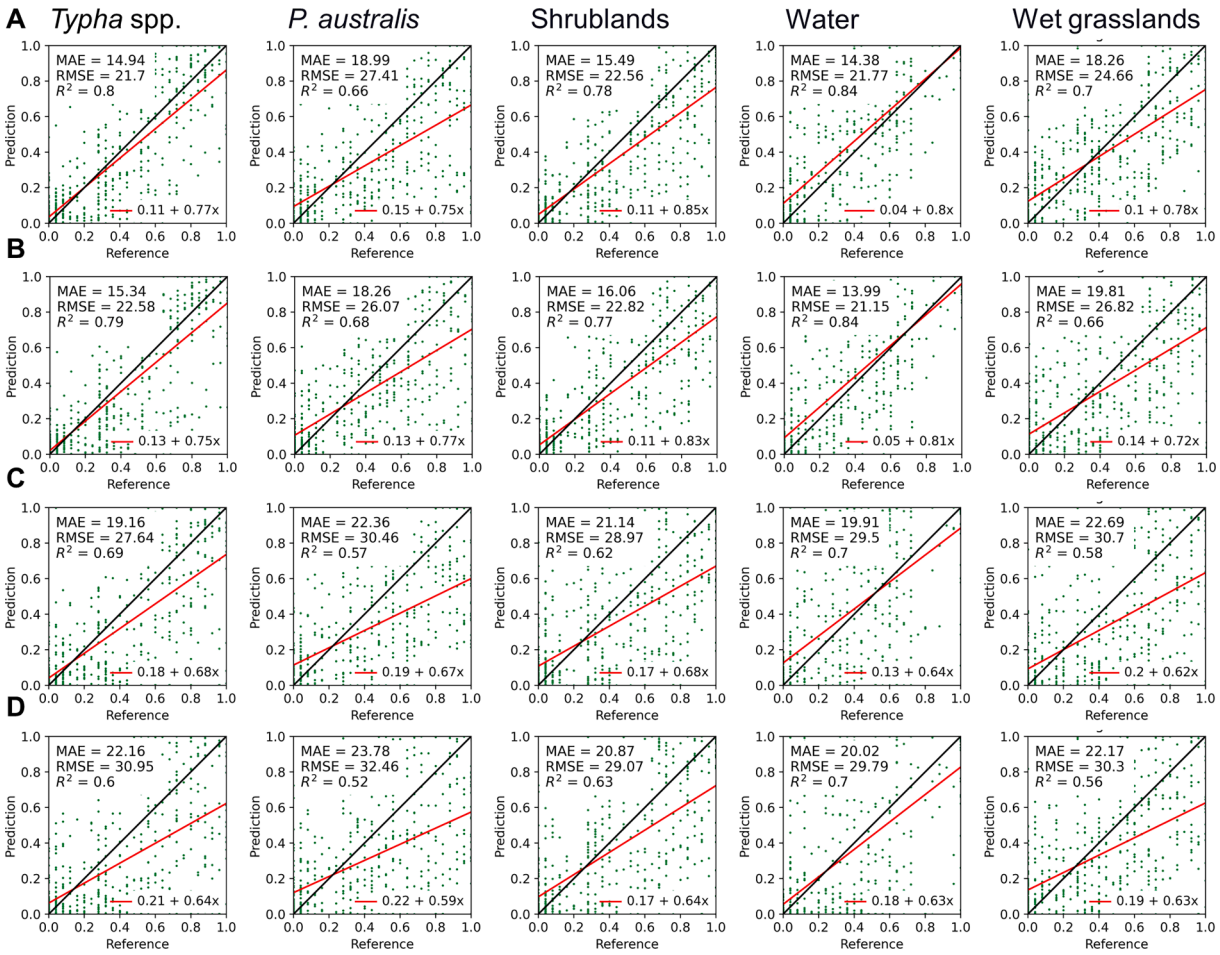

Fig. 7. The scatterplots of predicted vs. reference fractions. A) Unmixing results from PRISMA April-June, B) PRISMA April-June-August, C) Best pixel composite (April-June) of L8 and S2, and D) annual spectral-temporal metrics from L8 and S2.

data from these systems requires sub-pixel analyses to derive cover fractions of the relevant vegetation types. Our results indicate that PRISMA data can be used to generate highly accurate maps of peatland vegetation fractions. Such knowledge of, e.g., the water fraction, the proportion of various peatland species, and associated land cover information, can support paludiculture management by indicating the abundance of managed species but also by functioning as proxies for the rewetting success: Rewetting conditions, such as dry or wet conditions, are explained by transition zones between species and water fractions; this information also aids in preventing the expansion of shrublands into peatlands, as shrublands can invade peatlands when conditions are dry (Wichtmann and Schäfer, 2007). Additionally, fraction maps can be used to investigate the diversity and occupancy of various peatland taxa in protected areas.

The aim of this study was to investigate the contribution of data from new spaceborne imaging spectrometers to monitoring peatland vegetation cover, and this way, the success of rewetting activities. We specifically tested whether single-date or multi-date hyperspectral images are better for mapping vegetation fractions in peatlands (RQ1). We found that using multidate-observation hyperspectral datasets can provide a more accurate estimate than a single-date observation. The multi-date hyperspectral images accurately mapped the target class fraction of *Typha* spp. and *P. australis*. When single dates were compared, they all showed similar average MAE; however, the June data produced the best results for mapping *Typha* spp., whereas the April datasets produced the best mapping results for *P. australis*.

With regard to multi-date imagery, the April-June PRISMA datasets produced the best results (Table 2) in detecting *Typha* spp. (MAE = 14.94 %) compared to other combinations. The phenological variation between April-June (end of winter season – growing season) made a significant contribution to the best outcomes. Variation stems, e.g., from the unique *Typha* spp. cigar-shaped brown flowering that begins in May and ends in July (Demırezen and Aksoy, 2004; Heinz, 2011; Pijlman et al., 2019) and from the strong chlorophyll content in *P. australis* without any flower from May to June. The PRISMA April-June datasets, on the other hand, produced marginally more errors in identifying *P. australis* than the April-August datasets; we assume that the April-August datasets have the most promising results due to the presence of the red-purple *P. australis* flowers, which start blooming at the end of July and appear in August. (McKEE and Richards, 1996; Packer et al., 2017; Vymazal and Krőpfelová, 2005). The fraction results from three date combinations (April-June-August) produced the best average accuracy for both *P. australis* and *Typha* spp.

Given the fact that each peatland species' flowering and growth phases vary and that individual species have different best observation dates, the contribution of multi-date imagery can be clearly confirmed. This finding is in line with previous research using multispectral data (QuickBird), which also noticed that multiseason data gave the best results by incorporating phenological variation (Ghioca-Robrecht et al., 2008). When biomass is high, single-date imagery can show a similar spectral reflectance among the peatland species.

We achieved less than 19% overall MAE for mapping all classes using hyperspectral images and for some target classes clearly lower class-wise MAE. The point distribution in the scatter plots (Fig. 7) shows that despite some remaining offsets to the 1:1 line, the gradual distribution of LC fractions is represented in the results, which hence go beyond the

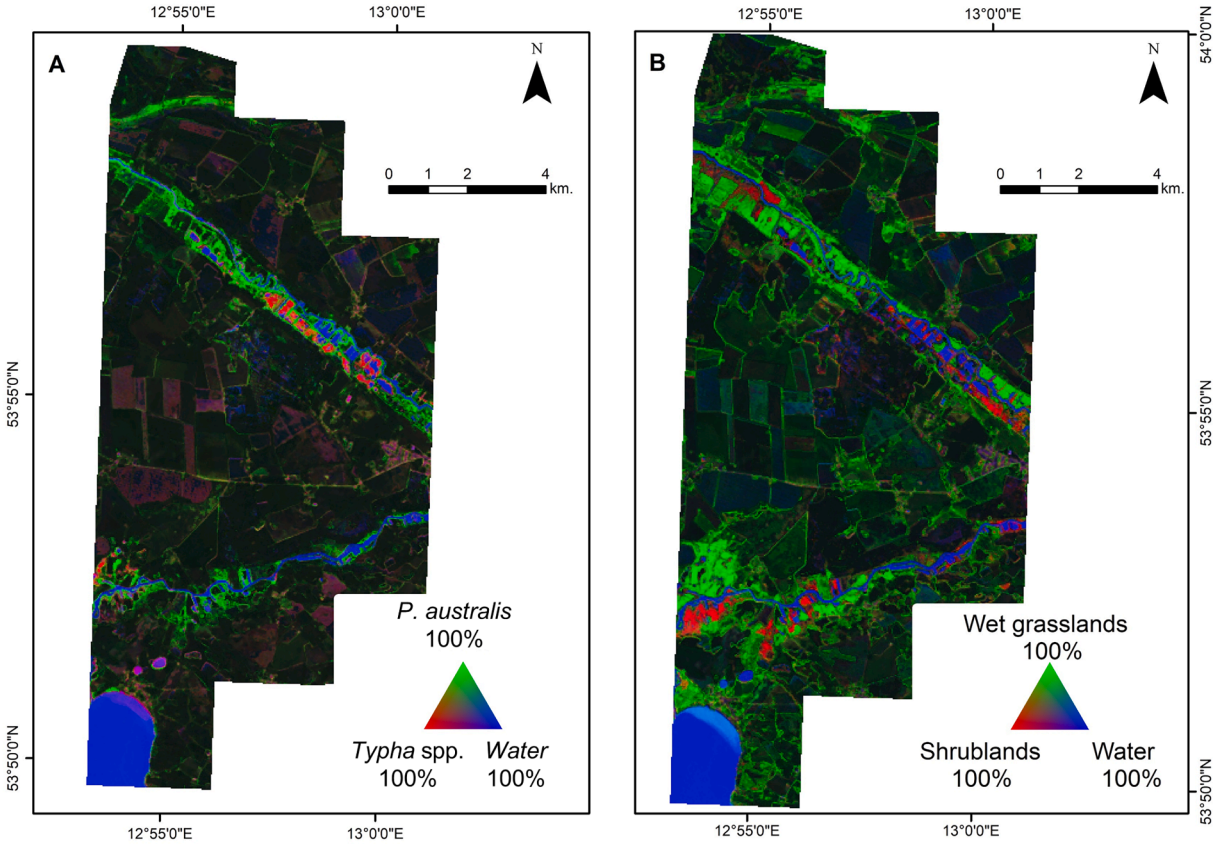

Fig. 8. Fraction maps based on the April-June PRISMA data for A) *P. australis*, *Typha* spp., and water, and B) shrublands, wet grasslands, and water.

information derived in a discrete LC classification. The correlation between prediction and reference is high (R^2 ~0.8 in most cases) when multiple observations of hyperspectral data are used, and the fitted line is close to the 1:1 line. Especially for models that achieve MAEs as low as ~15%, the high correlation is visible in the distribution of the point clouds. Here, the quantitative superiority of the hyperspectral to the multispectral results becomes clearly visible. Although results for *P. australis* were lower than for the other target classes, the MAE of 19% in a quantitative map of areal species fractions appears more accurate and higher in information content than, e.g., the 61.1.% class-wise accuracy of a discrete classification achieved in an existing study (Pengra et al., 2007). From a methods perspective, the regression-based unmixing approach (Okujeni et al., 2013) proved reliable for mapping the fraction of *P. australis* and *Typha* spp. with medium-resolution hyperspectral data. In accordance with Okujeni et al. (2021) we can report that the approach is capable of using the information from multi-date hyperspectral images, which leads to the highest accuracies for most LC fractions. Our study shows that the regression-based unmixing approach may even be used at the species level when multi-date hyperspectral images are used. The target species dominating in our study area, i.e., *P. australis* and *Typha* spp., existed both in rather pure patches and in transition zones (see Fig. 6). In contrast, *P. arundinacea* and *Carex* spp. were principally dispersed and did not appear in larger patches; therefore, no sufficient number of pure pixels were available for training and we were not able to map them individually using 30 m PRISMA datasets with the selected approach. Hence, we merged them as part of the wet grassland category. For future work, the inclusion of areas where these species are more widely available seems useful. Furthermore, the increasing availability of spaceborne hyperspectral data may lead to multi-date spectral libraries, e.g., incorporating spectral profiles from PRIMSA or EnMAP, but also higher resolution airborne data (Priem et al., 2019). These may then be used in studies targeting even more species.

Furthermore, we investigated the differences between results from hyperspectral and multispectral data for unmixing peatland vegetation communities (RQ2). Both single and multi-date hyperspectral datasets lead to higher accuracies than multispectral data from multiple observations. Our direct comparison was limited to the April-June two-date imagery, due to little coincidence in data availability for the two data types. Nevertheless, results of the direct comparison were 4–5% lower in MAE for the April-June PRISMA data, and even results from each single-data hyperspectral dataset were better in MAE by ~2% or more. Therefore, the additional spectral information content of the PRISMA data seems highly relevant for the quantitative description of peatland vegetation fractions.

The strength of multispectral data from L8 and S2 lies in the high temporal information content and hence the good representation of the phenological variation of plants, which may be represented in STM (Griffiths et al., 2019). Therefore, we additionally compared results from PRISMA to those from STM, which incorporate all cloud-free pixels from S2 and L8. The STM achieved the weakest accuracies during our experiments; however, the two-date multispectral data was more accurate than STMs. For example, the fraction results of *Typha* spp. (MAE = 19.16%) and *P. australis* (MAE = 22.36%) from the April-June multispectral datasets (Fig. 7) was slightly better than the fraction results of *Typha* spp. (ΔMAE + 3%) and *P. australis* (ΔMAE + 1%) from the annual STMs. It can be assumed that the phenological shift between April and June contributes to accuracies. But this shift is invisible in the STMs due to temporal aggregation.

Our work towards answering RQ 1 and 2 clearly shows that medium-resolution hyperspectral images (PRISMA) contribute to more accurate monitoring of vegetation composition in rewetted peatlands. We revealed differences in best observations for detecting different peatland species. Combining multiple hyperspectral observations produced the

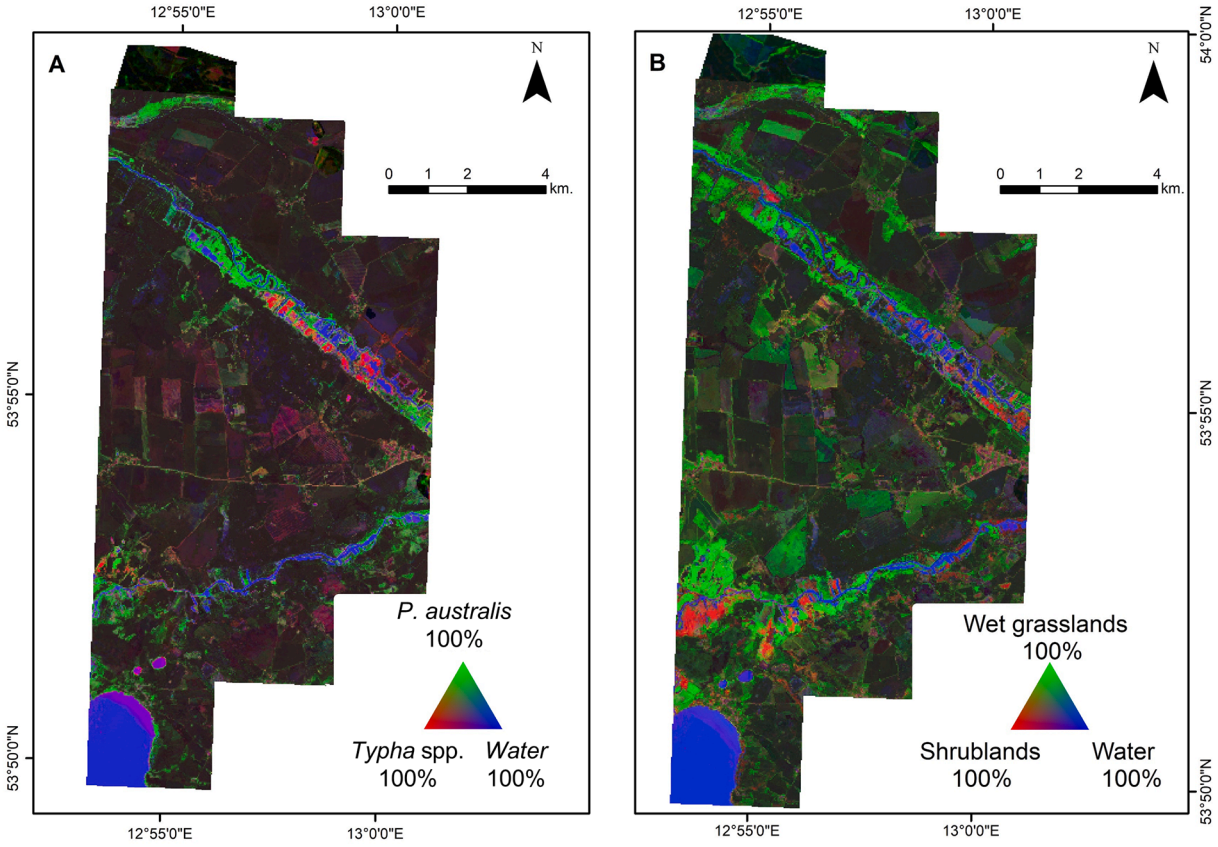

Fig. 9. Fraction maps based on April-June (best pixel composite) S2/L8 datasets for A) *P. australis*, *Typha* spp., and water, and B) shrublands, wet grasslands and water.

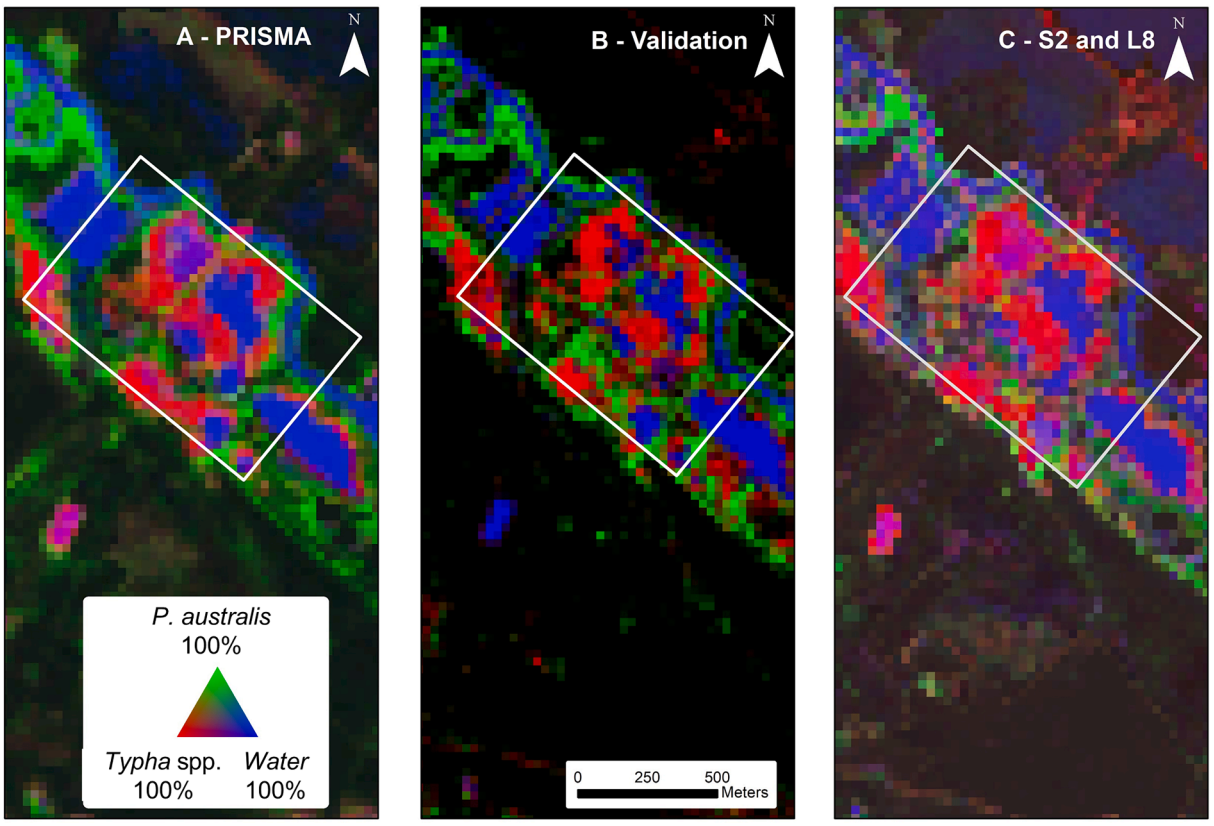

Fig. 10. A) The fraction map from PRISMA April-June, B) Validation data from AVIRIS-NG, and C) The fraction map from the S2 and L8 datasets (April-June BPC).

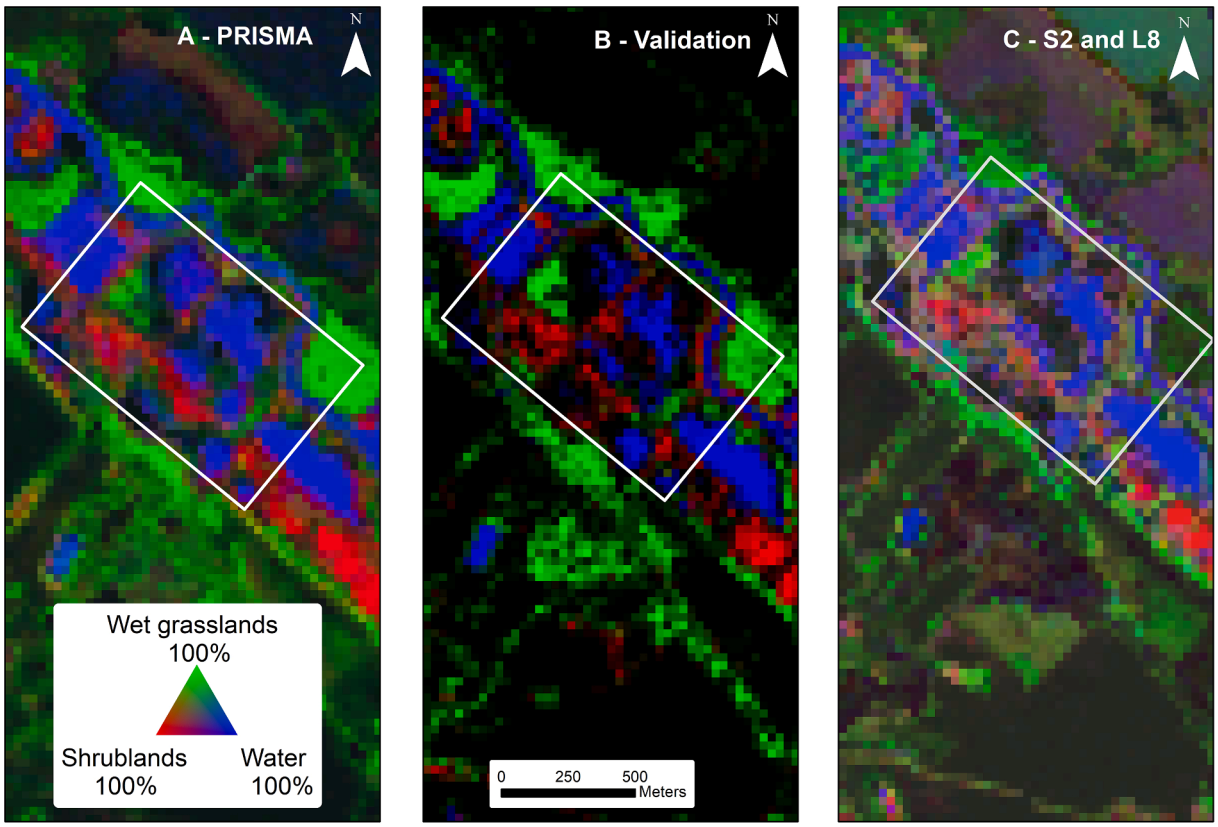

Fig. 11. A) The fraction map from PRISMA April-June, B) Validation data and C) The fraction map from the S2 and L8 datasets (April-June BPC).

most accurate LC fraction maps for all vegetation types. We can therefore clearly show a contribution of multi-date information. Still, it is unclear whether adding more data will further improve the accuracies for specific species and all LC fractions. Similarly, answering the question of optimal observation dates requires much denser data availability, which can, however, be expected with the parallel availability of multiple hyperspectral sensors in the future.

With regard to the benefits of the hyperspectral information compared to that from operational multispectral instruments, we could show the superiority of the hyperspectral data. Nevertheless, the data situation in 2021 did not allow for exploring the full potential of multispectral data. Here, further studies on combining the 30 m hyperspectral data with normally much denser S2 time series with 10 m resolution may be most interesting. Especially for less cloudy years, the S2 information will probably add more details. Despite the potentially better results from denser multispectral time series, the benefits of incorporating multi-date hyperspectral information into the monitoring of peatlands are very clear.

5. Conclusions

In the context of climate change mitigation, the monitoring of peatlands, their rewetting success and management can be expected to gain higher relevance in the near future. The quantification of peatland vegetation types and, more importantly, those species used in paludiculture schemes is one main component of this monitoring. We have shown that imagery from spaceborne hyperspectral sensors can contribute to such quantitative maps based on both, their multi-data availability and the high spectral information content compared to multispectral data. Therefore, we extend the application fields for this increasingly available data source by another highly relevant one. The quantitative description of peatland vegetation fractions is possible at high accuracies and hence goes clearly beyond that of discrete classification. For the application of spaceborne hyperspectral data in general, we have shown that in the future, the more frequent availability of the data marks a milestone in monitoring environmental processes intra-annually. Moreover, findings from this work underline the capabilities of regression-based unmixing with synthetically mixed training data in the context of deriving land cover fractions, even at a high level of thematic detail. In combination, the mapping approach in combination with the hyperspectral data can be expected to contribute to multiple environmental processes.

Declaration of Competing Interest

The authors declare that they have no known competing financial interests or personal relationships that could have appeared to influence the work reported in this paper.

Data availability

Data will be made available on request.

Acknowledgements

The Italian Space Agency (ASI) provided the ORIGINAL PRISMA Products for this research, which were delivered under an ASI License to Use. We are grateful to Planet's Education and Research Program for allowing us to use PlanetScope images during pre-processing. This research was conducted in the frame of the Interdisciplinary Research Center for the Baltic Sea Region Research (IFZO), University of Greifswald, Germany, and the research project Fragmented Transformation, which is funded by the German Federal Ministry of Education and Research (FKZ 01UC2102). We thank Carlos Rubio and Bernd Bobertz for their help with fieldwork and the two anonymous reviewers for their valuable feedback.

Appendix A. Supplementary data

Supplementary data to this article can be found online at https://doi.org/10.1016/j.ecolind.2023.110665.

References

Abeysinghe, T., Simic Milas, A., Arend, K., Hohman, B., Reil, P., Gregory, A., Vázquez-Ortega, A., 2019. Mapping invasive Phragmites australis in the Old Woman Creek estuary using UAV remote sensing and machine learning classifiers. Remote Sensing 11, 1380.

Atzberger, C., Rembold, F., 2013. Mapping the spatial distribution of winter crops at sub-pixel level using AVHRR NDVI time series and neural nets. Remote Sensing 5, 1335–1354.

Bain, C.G., Bonn, A., Stoneman, R., Chapman, S., Coupar, A., Evans, M., et al., 2011. IUCN U.K. commission of inquiry on peatlands. IUCN U.K. Peatland Programme, Edinburgh, United Kingdom.

Barthelmes, A., Couwenberg, J., Risager, M., Tegetmeyer, C., Joosten, H., 2015. Peatlands and climate in a ramsar context: a nordic-baltic perspective. Nordic Council of Ministers.

Beyer, F., Jurasinski, G., Couwenberg, J., Grenzdörffer, G., 2019. Multisensor data to derive peatland vegetation communities using a fixed-wing unmanned aerial vehicle. International Journal of Remote Sensing 40 (24), 9103–9125.

Beyer, F., Jansen, F., Jurasinski, G., Koch, M., Schröder, B., Koebsch, F., 2021. Drought years in peatland rewetting: rapid vegetation succession can maintain the net CO 2 sink function. Biogeosciences 18, 917–935.

Borges, J., Higginbottom, T.P., Cain, B., Gadiye, D.E., Kisingo, A., Jones, M., Symeonakis, E., Disney, M., Levick, S., 2022. Landsat time series reveal forest loss and woody encroachment in the Ngorongoro Conservation Area, Tanzania. Remote Sensing in Ecology and Conservation 8 (6), 808–826.

Brown, E., Aitkenhead, M., Wright, R., Aalders, I.H., 2007. Mapping and classification of peatland on the Isle of Lewis using Landsat ETM+. Scottish Geographical Journal 123 (3), 173–192.

Cooper, S., Okujeni, A., Jänicke, C., Clark, M., van der Linden, S., Hostert, P., 2020. Disentangling fractional vegetation cover: Regression-based unmixing of simulated spaceborne imaging spectroscopy data. Remote Sensing of Environment 246, 111856.

Curtis, C.J., Battarbee, R.W., Monteith, D.T., Shilland, E.M., 2014. The future of upland water ecosystems of the UK in the 21st century: A synthesis. Ecological indicators 37, 412–430.

Demırezen, D., Aksoy, A., 2004. Accumulation of heavy metals in Typha angustifolia (L.) and Potamogeton pectinatus (L.) living in Sultan Marsh (Kayseri, Turkey). Chemosphere 56 (7), 685–696.

Deutscher-Wetterdienst, 2023. Klimadaten f€ur Deutschland. Stan-dort Greifswald.

Dise, N.B., 2009. Peatland response to global change. Science 326 (5954), 810–811.

Elmer, K., Kalacska, M., Arroyo-Mora, J.P., 2021. Mapping the Extent of Invasive Phragmites australis subsp. australis From Airborne Hyperspectral Imagery. Frontiers in Environmental Science 9, 757871.

EnMAP-Box. EnMAP-Box 3-A QGIS Plugin to process and visualize hyperspectral remote sensing data. https://enmap-box.readthedocs.io/en/latest/.

Fluet-Chouinard, E., Stocker, B.D., Zhang, Z., Malhotra, A., Melton, J.R., Poulter, B., Kaplan, J.O., Goldewijk, K.K., Siebert, S., Minayeva, T., Hugelius, G., Joosten, H., Barthelmes, A., Prigent, C., Aires, F., Hoyt, A.M., Davidson, N., Finlayson, C.M., Lehner, B., Jackson, R.B., McIntyre, P.B., 2023. Extensive global wetland loss over the past three centuries. Nature 614 (7947), 281–286.

Fraixedas, S., Lindén, A., Meller, K., Lindström, Å., Keišs, O., Kålås, J.A., Husby, M., Leivits, A., Leivits, M., Lehikoinen, A., 2017. Substantial decline of Northern European peatland bird populations: Consequences of drainage. Biological conservation 214, 223–232.

Frantz, D., 2019. FORCE—Landsat+ Sentinel-2 analysis ready data and beyond. Remote Sensing 11, 1124.

Frantz, D., Haß, E., Uhl, A., Stoffels, J., Hill, J., 2018. Improvement of the Fmask algorithm for Sentinel-2 images: Separating clouds from bright surfaces based on parallax effects. Remote sensing of environment 215, 471–481.

Ge, Y., 2013. Sub-pixel land-cover mapping with improved fraction images upon multiple-point simulation. International Journal of Applied Earth Observation and Geoinformation 22, 115–126.

Ge, Y., Chen, Y., Stein, A., Li, S., Hu, J., 2016. Enhanced subpixel mapping with spatial distribution patterns of geographical objects. IEEE transactions on geoscience and remote sensing 54 (4), 2356–2370.

Ghioca-Robrecht, D.M., Johnston, C.A., Tulbure, M.G., 2008. Assessing the use of multiseason QuickBird imagery for mapping invasive species in a Lake Erie coastal marsh. Wetlands 28 (4), 1028–1039.

Görn, S., Fischer, K., 2015. Measuring the efficiency of fen restoration on carabid beetles and vascular plants: a case study from north-eastern Germany. Restoration Ecology 23 (4), 413–420.

Görn, S., Schulze, F., Fischer, K., 2015. Effects of fen management on bird communities in north-eastern Germany. Journal of Ornithology 156 (1), 287–296.

Griffiths, P., Nendel, C., Hostert, P., 2019. Intra-annual reflectance composites from Sentinel-2 and Landsat for national-scale crop and land cover mapping. Remote sensing of environment 220, 135–151.

Guanter, L., Kaufmann, H., Segl, K., Foerster, S., Rogass, C., Chabrillat, S., Kuester, T., Hollstein, A., Rossner, G., Chlebek, C., Straif, C., Fischer, S., Schrader, S., Storch, T., Heiden, U., Mueller, A., Bachmann, M., Mühle, H., Müller, R., Habermeyer, M., Ohndorf, A., Hill, J., Buddenbaum, H., Hostert, P., van der Linden, S., Leitão, P., Rabe, A., Doerffer, R., Krasemann, H., Xi, H., Mauser, W., Hank, T., Locherer, M., Rast, M., Staenz, K., Sang, B., 2015. The EnMAP spaceborne imaging spectroscopy mission for earth observation. Remote Sensing 7 (7), 8830–8857.

Günther, A., Barthelmes, A., Huth, V., Joosten, H., Jurasinski, G., Koebsch, F., Couwenberg, J., 2020. Prompt rewetting of drained peatlands reduces climate warming despite methane emissions. Nature communications 11, 1–5.

Haldan, K., Köhn, N., Hornig, A., Wichmann, S., Kreyling, J., 2022. Typha for paludiculture—Suitable water table and nutrient conditions for potential biomass utilization explored in mesocosm gradient experiments. Ecology and Evolution 12, e9191.

Heinz, S., 2011. Population biology of Typha latifolia L. and Typha angustifolia L.: establishment, growth and reproduction in a constructed wetland. Technische Universität München.

Hennicke, F., 2001. Das Naturschutzgroßprojekt 'Peenetal-Landschaft'. Landschaftsökologische Moorkunde 2, 487–492.

Higgisson, W., Cobb, A., Tschierschke, A., Dyer, F., 2021. Estimating the cover of Phragmites australis using unmanned aerial vehicles and neural networks in a semi-arid wetland. River Research and Applications 37, 1312–1322.

Hoffmann, H., Kleeberg, A., Görn, S., Fischer, K., Hassall, C., Barton, P., 2018. Riverine fen restoration provides secondary habitat for endangered and stenotopic rove beetles (Coleoptera: Staphylinidae). Insect Conservation and Diversity 11 (2), 194–203.

Joosten, H., Tanneberger, F., Moen, A., 2017. Mires and Peatlands of Europe. Status, Distribution and Conservation. Schweizerbart, Stuttgart.

Joosten, H., Sirin, A., Couwenberg, J., Laine, J., Smith, P., 2016. The role of peatlands in climate regulation, Peatland restoration and ecosystem services: science, policy and practice. In: Bonn, A., Allott, T., Evans, M., Joosten, H., Stoneman, R. (Eds.), Peatland Restoration and Ecosystem Services: Science, Policy and Practice. Cambridge University Press, Cambridge, UK, pp. 63–76.

Kattenborn, T., Lopatin, J., Förster, M., Braun, A.C., Fassnacht, F.E., 2019. UAV data as alternative to field sampling to map woody invasive species based on combined Sentinel-1 and Sentinel-2 data. Remote sensing of environment 227, 61–73.

Joosten, H., 2010. The global peatland CO2 picture. Peatland status and drainage related emissions in all countries of the world. Wetlands International, Wageningen. the Netherlands, p. 36.

Ke, G., Meng, Q., Finley, T., Wang, T., Chen, W., Ma, W., Ye, Q., Liu, T.Y., 2017. Lightgbm: a highly efficient gradient boosting decision tree. In: Guyon, I., Luxburg, U.V., Bengio, S., Wallach, H., Fergus, R., Vishwanathan, S., Garnett, R. (Eds.), Advances in neural information processing systems, vol. 30, pp. 3146–3154.

Kettridge, N., Turetsky, M.R., Sherwood, J.H., Thompson, D.K., Miller, C., Benscoter, B. W., Flannigan, M.D., Wotton, B., Waddington, J.M., 2015. Moderate drop in water table increases peatland vulnerability to post-fire regime shift. Scientific reports 5, 1–4.

Kimmel, K., Mander, Ü., 2010. Ecosystem services of peatlands: Implications for restoration. Progress in Physical Geography 34 (4), 491–514.

Knoth, C., Klein, B., Prinz, T., Kleinebecker, T., Goslee, S., 2013. Unmanned aerial vehicles as innovative remote sensing platforms for high-resolution infrared imagery to support restoration monitoring in cut-over bogs. Applied vegetation science 16 (3), 509–517.

KopeŁ, D., Michalska-Hejduk, D., Sławik, Ł., Berezowski, T., Borowski, M., Rosadziński, S., Chormański, J., 2016. Application of multisensoral remote sensing data in the mapping of alkaline fens Natura 2000 habitat. Ecological indicators 70, 196–208.

Krankina, O., Pflugmacher, D., Friedl, M., Cohen, W., Nelson, P., Baccini, A., 2008. Meeting the challenge of mapping peatlands with remotely sensed data. Biogeosciences 5, 1809–1820.

Kreyling, J., Tanneberger, F., Jansen, F., van der Linden, S., Aggenbach, C., Blüml, V., Couwenberg, J., Emsens, W.-J., Joosten, H., Klimkowska, A., Kotowski, W., Kozub, L., Lennartz, B., Liczner, Y., Liu, H., Michaelis, D., Oehmke, C., Parakenings, K., Pleyl, E., Poyda, A., Raabe, S., Röhl, M., Rücker, K., Schneider, A., Schrautzer, J., Schröder, C., Schug, F., Seeber, E., Thiel, F., Thiele, S., Tiemeyer, B., Timmermann, T., Urich, T., van Diggelen, R., Vegelin, K., Verbruggen, E., Wilmking, M., Wrage-Mönnig, N., Wołejko, L., Zak, D., Jurasinski, G., 2021. Rewetting does not return drained fen peatlands to their old selves. Nature communications 12 (1).

Lees, K., Quaife, T., Artz, R., Khomik, M., Clark, J., 2018. Potential for using remote sensing to estimate carbon fluxes across northern peatlands–A review. Science of the Total Environment 615, 857–874.

Lehosmaa, K., Jyväsjärvi, J., Virtanen, R., Ilmonen, J., Saastamoinen, J., Muotka, T., 2017. Anthropogenic habitat disturbance induces a major biodiversity change in habitat specialist bryophytes of boreal springs. Biological Conservation 215, 169–178.

Leifeld, J., Menichetti, L., 2018. The underappreciated potential of peatlands in global climate change mitigation strategies. Nature communications 9, 1–7.

Loizzo, R., Guarini, R., Longo, F., Scopa, T., Formaro, R., Facchinetti, C., Varacalli, G., 2018. PRISMA: The Italian hyperspectral mission, IGARSS 2018–2018 IEEE International Geoscience and Remote Sensing Symposium. IEEE 175–178.

Lupascu, M., Varkkey, H., Tortajada, C., 2020. Is flooding considered a threat in the degraded tropical peatlands? Science of the Total Environment 723, 137988.

McKEE, J., Richards, A., 1996. Variation in seed production and germinability in common reed (Phragmites australis) in Britain and France with respect to climate. New Phytologist 133, 233–243.

McPartland, M., Falkowski, M., Reinhardt, J., Kane, E., Kolka, R., Turetsky, M., Douglas, T., Anderson, J., Edwards, J., Palik, B., Montgomery, R., 2019. Characterizing boreal peatland plant composition and species diversity with hyperspectral remote sensing. Remote Sensing 11 (14), 1685.

Okujeni, A., van der Linden, S., Tits, L., Somers, B., Hostert, P., 2013. Support vector regression and synthetically mixed training data for quantifying urban land cover. Remote Sensing of Environment 137, 184–197.
Okujeni, A., van der Linden, S., Hostert, P., 2015. Extending the vegetation–impervious–soil model using simulated EnMAP data and machine learning. Remote Sensing of Environment 158, 69–80.
Okujeni, A., Jänicke, C., Cooper, S., Frantz, D., Hostert, P., Clark, M., Segl, K., van der Linden, S., 2021. Multi-season unmixing of vegetation class fractions across diverse Californian ecoregions using simulated spaceborne imaging spectroscopy data. Remote Sensing of Environment 264, 112558.
Packer, J.G., Meyerson, L.A., Skálová, H., Pyšek, P., Kueffer, C., 2017. Biological flora of the British Isles: Phragmites australis. Journal of Ecology 105 (4), 1123–1162.
Parish, F., Sirin, A., Charman, D., Joosten, H., Minayeva, T., 2008. Silvius. In: Stringer, L. (Ed.), Assessment on peatlands, biodiversity and climate change: main report. Global Environment Centre, Kuala Lumpur and Wetlands International, Wageningen, p. 179.
Pengra, B.W., Johnston, C.A., Loveland, T.R., 2007. Mapping an invasive plant, Phragmites australis, in coastal wetlands using the EO-1 Hyperion hyperspectral sensor. Remote Sensing of Environment 108 (1), 74–81.
Pepe, M., Pompilio, L., Gioli, B., Busetto, L., Boschetti, M., 2020. Detection and classification of non-photosynthetic vegetation from PRISMA hyperspectral data in croplands. Remote Sensing 12, 3903.
Pijlman, J., Guerts, J., Vroom, R., Bestman, M., Fritz, C., van Eekeren, N., 2019. The effects of harvest date and frequency on the yield, nutritional value and mineral content of the paludiculture crop cattail (Typha latifolia L.) in the first year after planting. Mires Peat 1–19. https://doi.org/10.19189/MaP.2017.OMB.325.
Pouliot, R., Rochefort, L., Karofeld, E., 2011. Initiation of microtopography in revegetated cutover peatlands. Applied Vegetation Science 14, 158–171.
Priem, F., Okujeni, A., van der Linden, S., Canters, F., 2019. Comparing map-based and library-based training approaches for urban land-cover fraction mapping from Sentinel-2 imagery. International Journal of Applied Earth Observation and Geoinformation 78, 295–305.
Roucoux, K.H., Lawson, I.T., Baker, T.R., Del Castillo Torres, D., Draper, F.C., Lähteenoja, O., Gilmore, M.P., Honorio Coronado, E.N., Kelly, T.J., Mitchard, E.T.A., Vriesendorp, C.F., 2017. Threats to intact tropical peatlands and opportunities for their conservation. Conservation Biology 31 (6), 1283–1292.
Saarinen, T., Celebi, A., Kløve, B., 2013. Links between river water acidity, land use and hydrology. Boreal Environment Research 18 (5), 359–372. Helsinki, Finland. Retrieved from https://helda.helsinki.fi/bitstream/handle/10138/229470/ber18-5-359.pdf?sequence=1.
Scheffler, D., Hollstein, A., Diedrich, H., Segl, K., Hostert, P., 2017. AROSICS: An automated and robust open-source image co-registration software for multi-sensor satellite data. Remote sensing 9, 676.
Schulte, M.L., McLaughlin, D.L., Wurster, F.C., Varner, J.M., Stewart, R.D., Aust, W.M., Jones, C.N., Gile, B., 2019. Short-and long-term hydrologic controls on smouldering fire in wetland soils. International Journal of Wildland Fire 28, 177–186.
Sirin, A.A., Medvedeva, M.A., Makarov, D.A., Maslov, A.A., Joosten, H., 2020. Multispectral satellite based monitoring of land cover change and associated fire reduction after large-scale peatland rewetting following the 2010 peat fires in Moscow Region (Russia). Ecological Engineering 158, 106044.
Stanimirova, R., Graesser, J., Olofsson, P., Friedl, M.A., 2022. Widespread changes in 21st century vegetation cover in Argentina, Paraguay, and Uruguay. Remote Sensing of Environment 282, 113277.
Steenvoorden, J., Limpens, J., Crowley, W., Schouten, M.G.C., 2022. There and back again: Forty years of change in vegetation patterns in Irish peatlands. Ecological Indicators 145, 109731.
Strack, M., 2008. Peatlands and climate change. IPS, International Peat Society.
Succow, M., 1971. Die Talmoore des nordostdeutschen Flachlandes, ein Beitrag zur Charakterisierung des Moortyps „Niedermoor “. Archiv für Naturschutz und Landschaftsforschung 11, 133–168.
Tanneberger, F., Moen, A., Barthelmes, A., Lewis, E., Miles, L., Sirin, A., Tegetmeyer, C., Joosten, H., 2021. Mires in Europe—Regional diversity, condition and protection. Diversity 13, 381.
Tanneberger, F., Birr, F., Couwenberg, J., Kaiser, M., Luthardt, V., Nerger, M., Pfister, S., Oppermann, R., Zeitz, J., Beyer, C., van der Linden, S., Wichtmann, W., Närmann, F., 2022. Saving soil carbon, greenhouse gas emissions, biodiversity and the economy: paludiculture as sustainable land use option in German fen peatlands. Regional Environmental Change 22, 69.
Timmermann, T., Margóczi, K., Takács, G., Vegelin, K., 2009. Restoring species-poor fen grasslands: the role of water level for early succession. Applied Vegetation Science 9, 241–250.
Tuukkanen, T., Stenberg, L., Marttila, H., Finér, L., Piirainen, S., Koivusalo, H., Kløve, B., 2016. Erosion mechanisms and sediment sources in a peatland forest after ditch cleaning. Earth Surface Processes and Landforms 41 (13), 1841–1853.
Vangi, E., D'Amico, G., Francini, S., Giannetti, F., Lasserre, B., Marchetti, M., Chirici, G., 2021. The new hyperspectral satellite PRISMA: Imagery for forest types discrimination. Sensors 21, 1182.
Vroom, R.J., Xie, F., Geurts, J.J., Chojnowska, A., Smolders, A.J., Lamers, L.P., Fritz, C., 2018. Typha latifolia paludiculture effectively improves water quality and reduces greenhouse gas emissions in rewetted peatlands. Ecological engineering 124, 88–98.
Vymazal, J., Krőpfelová, L., 2005. Growth of Phragmites australis and Phalaris arundinacea in constructed wetlands for wastewater treatment in the Czech Republic. Ecological engineering 25 (5), 606–621.
Wichtmann, W., Schäfer, A., 2007. Alternative management options for degraded fens – Utilisation of biomass from rewetted peatlands. In: Okruszko, T., Maltby, E., Szatylowicz, J., Swiatek, D., Kotowski., W. (Eds.), Wetlands: monitoring, modeling and management. Taylor & Francis Group, London, pp. 273–279.
Xu, J., Morris, P.J., Liu, J., Holden, J., 2018. Hotspots of peatland-derived potable water use identified by global analysis. Nature Sustainability 1, 246–253.
Zerbe, S., Steffenhagen, P., Parakenings, K., Timmermann, T., Frick, A., Gelbrecht, J., Zak, D., 2013. Ecosystem service restoration after 10 years of rewetting peatlands in NE Germany. Environmental management 51, 1194–1209.
Zhu, Z., Woodcock, C.E., 2012. Object-based cloud and cloud shadow detection in Landsat imagery. Remote sensing of environment 118, 83–94.